

Supernova Feedback in Molecular Clouds: Global Evolution and Dynamics

Bastian Körtgen^{1*}, Daniel Seifried², Robi Banerjee¹, Enrique Vázquez–Semadeni³, and Manuel Zamora–Avilés³

¹ *Hamburger Sternwarte, Universität Hamburg, Gojenbergsweg 112, 21029 Hamburg, Germany*

² *I. Physikalisches Institut, Universität zu Köln, Zùlpicherstraße 77, 50937 Köln, Germany*

³ *Instituto de Radioastronomía y Astrofísica, Universidad Nacional Autónoma de México, Campus Morelia, Apdo. Postal 3-72, Morelia, 58089, México*

Released 2015

ABSTRACT

We use magnetohydrodynamical simulations of converging warm neutral medium flows to analyse the formation and global evolution of magnetised and turbulent molecular clouds subject to supernova feedback from massive stars. We show that supernova feedback alone fails to disrupt entire, gravitationally bound, molecular clouds, but is able to disperse small-sized (~ 10 pc) regions on timescales of less than 1 Myr. Efficient radiative cooling of the supernova remnant as well as strong compression of the surrounding gas result in non-persistent energy and momentum input from the supernovae. However, if the time between subsequent supernovae is short and they are clustered, large hot bubbles form that disperse larger regions of the parental cloud. On longer timescales, supernova feedback increases the amount of gas with moderate temperatures ($T \approx 300 - 3000$ K). Despite its inability to disrupt molecular clouds, supernova feedback leaves a strong imprint on the star formation process. We find an overall reduction of the star formation efficiency by a factor of 2 and of the star formation rate by roughly factors of 2–4.

Key words: magnetohydrodynamics (MHD) – turbulence – ISM: clouds – ISM: kinematics and dynamics

1 INTRODUCTION

The formation of molecular clouds, dense clumps, and finally stars is regulated by the interplay of gravity, magnetic fields, stellar feedback, and turbulence.

The effect of turbulence is two-fold. Firstly, in the cold neutral medium (CNM) turbulent fluctuations are primarily supersonic. Thus, shocks occur, which compress the gas and hence provide the seeds for gravitationally unstable regions (e.g. Mac Low & Klessen 2004). On the other hand, these supersonic motions constitute an effective pressure. This turbulent pressure acts as further support against gravity beside thermal and magnetic pressure. If the turbulence is also superalfvénic, it is the major support in molecular clouds (Padoan et al. 1999; Padoan & Nordlund 1999; Federrath & Klessen 2012, 2013).

Additionally the internal cloud dynamics are mediated by stellar feedback via jets/outflows, winds, ionising radiation, and supernovae. The role of jets and outflows is still being

subject to strong debate. On the one hand, they are able to drive turbulence in the intra-clump medium (Nakamura & Li 2014; Li et al. 2015a) and hence maintain the level of energy counterbalancing gravity. On the other hand, Banerjee et al. (2007) argue that the turbulent fluctuations, driven by a single source, are damped too fast as primarily compressive modes are excited. However, the combined effect of *multiple* outflows seems to be able to disperse (not disrupt) the parental clump (Banerjee et al. 2007; Wang et al. 2010; Nakamura & Li 2014).

Stellar winds are believed to have a stronger impact on the massive star’s environment and hence the parental cloud. As Dale et al. (2013) point out, winds are most efficient in dispersing dense, massive cores in which the stars are embedded. Their longrange impact, however, is not sufficient. Dale et al. (2014) compared simulations of idealised molecular clouds including stellar winds or ionisation feedback. The main driver of cloud dispersion is the massive star’s ionising radiation, consistent with studies by Vázquez–Semadeni et al. (2010). Stellar winds, in contrast, only help to shape the emerging HII regions. In detail, the emerging HII re-

* bkoertgen@hs.uni-hamburg.de

gions are more spherical and stable against shell instabilities. However, the efficiency of dispersing entire (giant) molecular clouds by these two feedback mechanisms strongly depends on the cloud’s mass and escape velocity. Concerning the impact of these mechanisms on the star formation process, Dale et al. (2014) and Vázquez-Semadeni et al. (2010) come to similar conclusions: ionisation feedback is most efficient in dispersing small regions. In addition, Colín et al. (2013) give a timescale for the dispersion of such regions (of size ~ 10 pc) of $t \approx 10 - 15$ Myr.

On scales of entire molecular clouds ionisation feedback may also help to trigger the formation of new stars (Gritschneider et al. 2009; Walch et al. 2012, 2013). However, the star formation efficiency is *globally* still being reduced by a factor of 10–20% but not halted (Dale et al. 2014). The degree of turbulence within the dense gas, in contrast, is only essential for the inhomogeneity of the cloud and hence the ability of the hot, ionised gas to escape through low-density channels. Finally, massive stars explode in a violent supernova event, thereby releasing $E_{\text{SN}} = 10^{51}$ erg in a short period of time. A number of studies exist that either focus on Galactic scales, (Rosen & Bregman 1995; Korpi et al. 1999; de Avillez 2000; de Avillez & Mac Low 2002; de Avillez & Breitschwerdt 2004; Joung & Mac Low 2006, 2007; Shetty & Ostriker 2008; Joung et al. 2009; Ostriker & Shetty 2011; Hill et al. 2012; Shetty & Ostriker 2012; Gent et al. 2013a,b; Walch et al. 2014; Hennebelle & Iffrig 2014; Gatto et al. 2015), or on scales of small clouds or even clumps with radii of a few pc (Pittard & Rogers 2012; Rogers & Pittard 2013; Walch & Naab 2015; Iffrig & Hennebelle 2015; Geen et al. 2015; Kim & Ostriker 2015).

Recently, Walch & Naab (2015) have reported on supernova feedback in small-sized (radius $r = 16$ pc), massive ($M \approx 10^5 M_{\odot}$) and non-magnetised molecular clouds. The authors injected momentum in a small sub-volume of the cloud in order to mimic the free-expansion phase of the supernova remnant (SNR). They resolved the different stages during the SNR evolution and analysed the influence of different physical mechanisms on this. For adiabatic expansion of the SNR in a homogeneous cloud, they yielded the complete dispersion of the latter on timescales of $t \leq 1$ Myr. However, the clouds – homogeneous or fractal – are *not being destroyed* if radiative cooling is included. The hot and shock-compressed gas cools too fast. Hence, the thermal energy supply, which can be converted into kinetic energy, shrinks on the same timescales. The net energy and momentum input are thus not sufficient to accelerate the gas to velocities greater than the cloud’s escape velocity. Similar results were obtained by Iffrig & Hennebelle (2015), who analysed the impact of supernova explosions within or near molecular clouds. The authors deduced that the impact of supernova feedback is primarily determined by the position of the progenitor star. Supernovae at the border of or near to a molecular cloud do not have a significant impact on a possible cloud dispersal as well as on the dynamics of the dense gas which is due to the lack of momentum transfer to the latter. The major part of the cloud is compressed and some regions are ablated. In the case of a supernova going off within a molecular cloud, the momentum transfer to the dense gas is much higher and hence the fraction of gas escaping the cloud. The results indicate a reduction of the cloud mass due to single supernova explosions of up to 50% for

clouds with masses of $M \approx 10^4 M_{\odot}$ and sizes of approximately 20–30 pc. However, the authors report no complete cloud dispersion.

Kim & Ostriker (2015) analysed supernova explosions in a two-phase ISM (see also a similar study by Martizzi et al. 2015). The authors found that the net momentum input from supernovae is nearly independent of the morphology of the environment and may only change if further feedback prior to the supernova is considered (see also Walch & Naab 2015).

In studies of Galactic scale simulations supernova feedback is usually taken into account since it is the main driver of Galactic fountain flows (e.g. Hill et al. 2012; Gent et al. 2013b; Walch et al. 2014, but see Girichidis et al. (2015) for details about the efficiency in launching these outflows). Usually, $E_{\text{SN}} = 10^{51}$ erg are injected during each individual supernova event. However, some approaches inject $E_{\text{SN}} = (2 - 3) \times 10^{51}$ erg in order to resemble additional energy input from ionisation and winds in one single event (P.Colín, priv. communication, 2012). Studies implementing more than one supernova are restricted to a certain supernova rate. For example, Joung & Mac Low (2006) use the *observed Galactic rate* of $\nu_{\text{SN,gal}} = 1/44 \text{ yr}^{-1}$ from Tammann et al. (1994). More recent studies by Walch et al. (2014) and Gatto et al. (2015) use a Kennicutt–Schmidt relation in order to extract the star formation rate surface density, Σ_{SFR} , and transform it to a supernova rate by convolution with an IMF.

Gatto et al. (2015) conducted a large parameter study of supernova feedback on Galactic scales. They investigated the influence of different supernova driving mechanisms on the thermal and dynamical state of the interstellar medium (ISM). Most relevant are their results from ‘peak driven’ supernovae – i.e. the supernovae exploded in regions of significantly enhanced density – which state that this driving mechanism fails to explain the large fraction of molecular gas as well as the volume filling fraction of hot, ionised gas. The former is most likely due to disruption of dense, cold branches by the interaction of the SNR with the densest gas. The latter originates in very efficient cooling of hot gas in the shock-compressed regions within the dense clumps. The gas temperatures are cooled efficiently to $T < 10^6$ K. This is supported by Walch et al. (2014), who yield realistic disc structure and volume filling fractions of the hot gas for non-peak driven supernovae. Both studies underline the importance of feedback mechanisms prior to supernova feedback. In addition, recent investigations by Li et al. (2015b) have shown that the volume filling fraction of the hot component of the ISM needs to be $f_V \sim 0.6$ in order to induce thermal runaway. In this case, the bubbles created by multiple supernovae connect to each other. In the contrary case of $f_V < 0.6$, the bubbles of supernova remnants do not connect and cooling dominates.

Our study bridges the gap between small-scale, i.e. 1 to a few 10 pc, simulations (Pittard & Rogers 2012; Walch & Naab 2015; Iffrig & Hennebelle 2015) and large-scale (kpc) disc simulations (Korpi et al. 1999; Ostriker & Shetty 2011; Walch et al. 2014; Tasker et al. 2015) by performing a set of simulations on intermediate scales of a few hundred pc. Section 2 introduces the numerical model as well as the initial conditions. The following section 3 gives the results of our study on supernova feedback, thereby focussing on the

global evolution of the (dense) gas. In section 4 we briefly discuss the limitations of our model. The study closes with a summary in section 5.

2 NUMERICAL SETUP AND INITIAL CONDITIONS

2.1 Details of the numerics

For this study we use the finite volume adaptive mesh-refinement (AMR) code FLASH (version 2.5) (Fryxell et al. 2000; Dubey et al. 2008). The code solves the ideal MHD equations, the Poisson equation for self-gravity of the gas, as well as heating and cooling. The MHD fluxes are computed by a multiwave Riemann solver developed by Bouchut et al. (2007, 2009) and implemented in FLASH by Waagan et al. (2011), which preserves positive states for density and internal energy. Since we are interested in the process of star formation, we also include sink particles to follow collapsing regions (Federrath et al. 2010). In order to form a sink particle, the gas has to pass several checks, which are described in detail in Federrath et al. (2010). Beside these checks, the density has to exceed a threshold density of $n_{\text{sink}} = 3 \times 10^5 \text{ cm}^{-3}$. Periodic boundary conditions (BCs) are applied for the hydrodynamics and self-gravity is treated with isolated BCs. Refinement of certain regions is achieved by resolving the local Jeans length with 10 grid cells, hence a factor of 2.5 larger than the usual Truelove criterion (Truelove et al. 1997), except at the maximum refinement level where it is still resolved with four grid cells.

2.2 Initial Conditions

Our numerical setup is adapted from Vázquez-Semadeni et al. (2007, see also Banerjee et al. (2009), Vázquez-Semadeni et al. (2011), and Körtgen & Banerjee (2015)). The physical size of the numerical box is $L_{\text{box}} = 256 \text{ pc}$. Two cylindrical flows of warm neutral medium (WNM) collide at the centre of the domain. Each flow has a linear dimension of $l = 112 \text{ pc}$ and a radius of $r = 64 \text{ pc}$. A schematic picture of the initial setup is shown in Körtgen & Banerjee (2015, see their figure 1). We have chosen the initial density to be $n = 1 \text{ cm}^{-3}$ and the temperature as $T = 5000 \text{ K}$, typical for the WNM. The total mass in the flows is $M_{\text{flows}} = 90,000 M_{\odot}$. The respective column density is $N_{\text{flows}} = 6.9 \times 10^{20} \text{ cm}^{-2}$. The sound speed at the given temperature is $c_s = 5.7 \text{ km/s}$, which we take as a reference speed. The mean molecular weight is $\mu = 1.27$. We choose the speed of the colliding flows such that the *isothermal* Mach number is $\mathcal{M}_{\text{flow}} = 2$. The dynamical time of each flow is thus $t_{\text{flow}} = L_{\text{flow}}/v_{\text{flow}} = 9.6 \text{ Myr}$. In addition we add a turbulent velocity field to the flows to mimic the general turbulent behavior of the ISM (Mac Low & Klessen 2004). The turbulent fluctuations are calculated in Fourier space with a Burgers type spectrum, i.e. $E(k) \propto k^{-2}$ for $k \geq k_{\text{int}}$, where k_{int} is the wave number of the integral scale ($\lambda_{\text{int}} = 64 \text{ pc}$). Furthermore, these turbulent fluctuations trigger the onset of dynamical instabilities such as the non-linear thin-shell instability (NTSI, Vishniac 1994) or the Kelvin-Helmholtz instability (e.g. Heitsch et al. 2005, 2008). The initially uniform magnetic field has a strength of $|\underline{B}| = 3 \mu\text{G}$ and is

Table 1. List of performed simulations, showing the simulation name in column one, the *isothermal* sonic Mach number in column two. In the third column we list the isothermal sonic Mach number. The last two columns show the initial magnetic field strength and the peak resolution, respectively.

Run Name	$\mathcal{M}_{\text{flow}}$	$\mathcal{M}_{\text{turb}}$	Feedback?	$ \underline{B} $ (μG)	Min. Δ (pc)
HR0.8N	2	0.8	No	3	0.03
HR0.8Y	2	0.8	Yes	3	0.03
HR1.0N	2	1.0	No	3	0.03
HR1.0Y	2	1.0	Yes	3	0.03
HR1.2N	2	1.2	No	3	0.03
HR1.2Y	2	1.2	Yes	3	0.03
HR0.8HN	2	0.8	No	0	0.03
HR0.8HY	2	0.8	Yes	0	0.03

aligned with the flows, that is, $\underline{B} \propto \hat{x}$ where \hat{x} is the unit vector in the x direction. Using the description for the critical mass-to-flux ratio by Nakano & Nakamura (1978), i.e. $\mu_{\text{crit}} = 0.16/\sqrt{G}$, the two streams are in total initially subcritical ($\mu/\mu_{\text{crit}} = 0.97$), but can become supercritical very fast due to accretion of mass along the field lines. We use a maximum refinement level of $\mathcal{L}_{\text{max}} = 11$, which corresponds to a maximum physical resolution of $\Delta x_{\text{max}} \approx 0.03 \text{ pc}$. A detailed overview of the simulation runs is given in table 1. The main parameters are summarised as follows:

- Flow mass: $M_{\text{flows}} = 90,000 M_{\odot}$
- Column density: $N_{\text{flows}} = 6.9 \times 10^{20} \text{ cm}^{-2}$
- Sound speed: $c_s = 5.7 \text{ km/s}$
- Box size: $L_{\text{box}} = 256 \text{ pc}$
- Maximum resolution: $\Delta x_{\text{max}} \approx 0.03 \text{ pc}$.

2.3 The supernova subgrid model

The supernova (SN) feedback is directly coupled to the sink particles¹. A Kroupa-IMF (Kroupa 2001) is fitted to the *total sink particle mass* each timestep in order to evaluate the number of massive stars within the cloud. The analytical evaluation of the IMF results in a minimum (or critical) mass $M_{\text{Kroupa}} = 160 M_{\odot}$ in order to form a massive star of mass $M_* \geq 10 M_{\odot}$. The SN model is only being activated if the total mass in all sink particles exceeds M_{Kroupa} . We then let the *most massive* sink particle explode in case:

- The particle has accreted at least $M_{\text{sink}} \geq 30 M_{\odot}$.
- The sink particle's life time is $t_{\text{lifetime}} \geq 2 \text{ Myr}$ according to standard mass-lifetime relations (Weigert et al. 2009).

These two criteria ensure that feedback is not being initiated before the mass and lifetime correspond to these of an O-type star. Although it is more likely to form a B-star with such a small mass reservoir, the respective lifetime would be too long (50 Myr) to affect molecular clouds via supernova feedback during their lifetime (20–30 Myr,

¹ For a resolution study we refer the reader to the appendix.

Blitz et al. 2007). Once, these two criteria are fulfilled, $E_{\text{SN}} = 10^{51}$ erg – with $E_{\text{th}} = 0.65 E_{\text{SN}}$ and $E_{\text{kin}} = 0.35 E_{\text{SN}}$ – are injected into a spherical control volume (CV, with a radius of $\mathcal{R}_{\text{CV}} = 0.06$ pc), similar to the original solution by Sedov (1959). The thermal energy is adjusted by increasing the pressure in the cells within the CV and the respective velocity increases radially with distance from the centre of the CV. We point out that in case of a SN going off the cooling time of the dense gas is still 6–7 times longer than the sound crossing time of the hot ($T \sim 10^6$ K) gas. Right after the SN energy is injected, the timestep of the simulation is automatically adjusted according to the Courant condition so that the fast pressure waves and the momentum input are properly resolved. The mass of the exploding star is uniformly mapped back onto the numerical grid. Sink particles, which have gone off as a SN become passive particles, that is, accretion is switched off and they do not feed back onto the gas a second time (i.e. if they still possess more than $30 M_{\odot}$). Passive particles are not considered anymore for the M_{Kroupa} -criterion.

If more than one massive star exists (i.e. $M_{\text{Sinks}}/M_{\text{Kroupa}} > 1$), the supernovae explode according to the criterion: one SN per $44 M_{\odot}$ of stars. This criterion is deduced from the SN type II rate of $1/44 \text{ yr}^{-1}$ (Tammann et al. 1994) and the average star formation rate of $\sim 1 M_{\odot} \text{ yr}^{-1}$ in the Milky Way (see e.g. Robitaille & Whitney 2010, and references therein). In such cases it is *the most massive* particle that explodes. Multiple massive stars are then not allowed to go off as a SN during subsequent timesteps until the total mass in sink particles has grown by $44 M_{\odot}$ compared to the mass at the time of the last SN. Note that this rate is higher than typical rates estimated from IMF calculations and thus gives an upper limit on the efficiency of supernova feedback. Note further that we do not include type I supernovae due to their low rate (see e.g. Tammann et al. 1994).

2.4 Heating and cooling

The ISM is subject to various heating and cooling processes, which affect the thermodynamic behaviour of the gas. Hence, heating and cooling are included as source terms in the energy equation. They are incorporated following the recipe by Koyama & Inutsuka (2000, with modifications by Vázquez-Semadeni et al. (2007)). This prescription results in a thermally unstable regime in the density range $1 \text{ cm}^{-3} \leq n \leq 10 \text{ cm}^{-3}$, corresponding to a temperature interval of $500 \text{ K} \leq T \leq 5000 \text{ K}$ if thermal equilibrium conditions are applied.

The fitting functions for heating, Γ , and cooling, Λ , give

$$\Gamma = 2.0 \times 10^{-26} \text{ erg s}^{-1} \quad (1)$$

$$\frac{\Lambda(T)}{\Gamma} = 10^7 \exp\left(\frac{-1.184 \times 10^5}{T + 1000}\right) \quad (2)$$

$$+ 1.4 \times 10^{-2} \sqrt{T} \exp\left(\frac{-92}{T}\right) \text{ cm}^3.$$

We remark that the cooling function stays almost constant for typical temperatures within supernova remnants ($T \geq 10^6$ K).

3 RESULTS

In the following we will present the results of this study. The focus will be on the global evolution of the molecular cloud and its resulting dynamics. The impact of supernova feedback on the process of star formation is being investigated in one of the last results sections.

3.1 Evolution of cloud masses

The left panel in figure 1 shows the evolution of the mass of the *clouds*. As a *cloud* in the simulations we define the regions with density of $n \geq 100 \text{ cm}^{-3}$, which must not necessarily be spatially connected. These clouds have a mean temperature of ~ 30 K. The decrease of dense gas mass between 8 and 17 Myr in the MHD runs is a consequence of the re-expansion of the compressed material (see e.g. Körtgen & Banerjee 2015, and references therein). For the hydrodynamic runs this stage is from 5 to 12 Myr and is thus faster. This is because of the lack of a magnetic field, which would decelerate the gas. After this stage (from 12 Myr in the hydrodynamic case and from 17 Myr on in the MHD case), global contraction of the cloud leads to an increase of mass (see also Banerjee et al. 2009). Generally the clouds are more massive for the hydrodynamic runs due to the lack of magnetic support. However, the accretion properties of the clouds seem very similar in the later stages from 20 Myr on, as can be inferred from the increase of their masses. These stages are independent of the initial conditions since the flows have vanished and the initial turbulence has fully decayed. In the end, the clouds have masses between $M_{\text{cloud}} = 2 \times 10^4 - 4 \times 10^4 M_{\odot}$. The difference of the cloud masses for the MHD runs is due to the fact that initially the stronger turbulence disperses the gas more efficient. This also prevents the build up of a massive cloud.

The impact of supernova feedback on the clouds is two-fold. On the one hand, the first supernova explosion results in a compression of the surrounding gas, thereby *increasing* the total mass of the dense gas. On the other hand, this period of compression lasts only until the point, where parts of the clouds are heated up and dispersed by the transmitted shocks. The increase of the mass depends on where the supernova goes off, that is, either in a compact or a structured environment (see also Iffrig & Hennebelle 2015). For example, Li et al. (2015b) point out that supernovae going off in a structured environment do interact with the high-density regions, but the long-term impact of the remnant is primarily onto the low-density medium. A supernova going off in a structured environment sweeps up less mass as its counterpart going off in a compact/homogeneous medium of same average density. For runs HR0.8Y and HR0.8HY, the cloud is compact enough to provide a significant obstacle to the emerging shock wave. An increase of mass is also seen in the cloud of run HR1.2Y, although the increase takes a longer time. In contrast, the supernova explosion in run HR1.0Y results in only a small increase of a few hundred solar masses. The denser regions are not significantly compressed. From the stage of dispersion of parts of the cloud on, the cloud mass stays lower in comparison to the clouds without feedback. If more and more supernovae go off, the growth in mass is either stopped or turned into a stage of decreasing mass (as in case HR1.0Y). The total decrease in

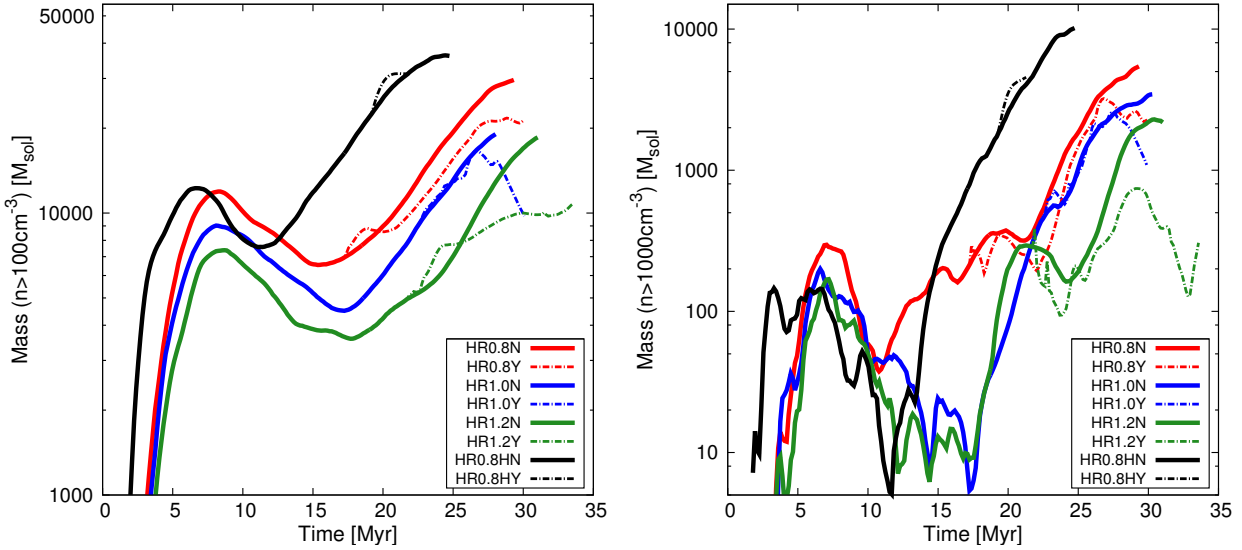


Figure 1. Temporal evolution of the mass of the cloud (left, $n \geq 100 \text{ cm}^{-3}$) and the densest parts in the cloud interior (right, $n \geq 1000 \text{ cm}^{-3}$). The data are evaluated within a cylindrical volume of radius $r = 50 \text{ pc}$ and height $h = 40 \text{ pc}$. Solid lines denote the runs without feedback, dash-dotted lines those with feedback. After the converging flows have vanished (at $t \approx 10 \text{ Myr}$) global collapse is initiated and the clouds become more massive. Note the different evolution of the cloud and the densest parts for HR0.8, respectively. Supernova feedback has a two-fold impact on the global evolution of the cloud mass (see text).

cloud mass is between a factor of 1.5–2, in agreement with a previous study by Iffrig & Hennebelle (2015). However, the efficiency of supernova feedback, that is, its impact onto the dense gas (e.g. reduction of the total gas mass), depends on the initial turbulence within the flows and thus the final cloud mass and (mean) density. Please note that the negligible difference in the cloud mass in runs HR0.8HN and HR0.8HY is coincidental and may increase with continuation of the simulation.

3.1.1 Evolution of the densest parts

In the right panel of figure 1 we present the evolution of the densest parts of the molecular cloud with densities of $n \geq 1000 \text{ cm}^{-3}$. The evolution of the densest parts is similar to the evolution of the cloud. The strong fluctuations during the early stages indicate that these regions are diluted due to the energy injection from the WNM flows and turbulence. All clouds undergo a lateral expansion phase (from $\sim 7 \text{ Myr}$) during which the amount of high-density gas decreases. However, the densest regions in run HR0.8N do not show such variation. The more compact cloud interior is nearly unaffected by the re-expansion of the cloud and keeps on accreting. The later evolutionary stages of all clouds – from 15 Myr on for the hydro case and from 17 Myr on for the MHD simulations – are dominated by global cloud contraction. Nevertheless, some of the high-density material can still be dispersed by the momentum injection and turbulence delivered by the colliding streams. The supernova explosions yield periods of varying total mass in the densest parts. This is due to dilatational and compressive stages and is seen in all runs. In the end, the mass of the densest parts in the MHD runs is reduced by factors of about three for HR0.8Y and HR1.0Y to of about ten for HR1.2Y.

3.2 Cloud Dynamics

Figure 2 shows a temporal sequence of the column density, temperature and total velocity for run HR0.8Y. The first row shows the molecular cloud 30 kyr *before* the first supernova, the other two rows after supernovae have gone off. Prior to the first supernova, the cloud reveals a filamentary network and clumps as well as low-density cavities in between. This is a result of the interaction of turbulence and gravity, mediated by the ambient magnetic field (e.g. Hennebelle 2013; Chen & Ostriker 2014; Körtgen & Banerjee 2015). The filaments are best being identified in the temperature slice as the cold branches with temperatures of about $T = 30 \text{ K}$, immersed in a warm medium with $T = 1000 - 5000 \text{ K}$.

The supernovae act only locally since the shock terminates after $\sim 15 \text{ pc}$. The cold, dense gas is redistributed, as is best seen in the temperature slices. In addition, the column density map before the first supernova and at the end of the simulation reveal different patterns at the cloud outskirts. Prior to supernova feedback, the outer border of the cloud is more spherical. After supernova feedback, the outskirts are more structured and the density of the WNM halo surrounding the cloud is higher. These parts of the molecular cloud do also reveal a slower inward-directed velocity, as can be identified from the length and orientation of the velocity vectors in the velocity pattern. Figure 3 shows the final stage of runs HR1.0N, HR1.0Y, HR1.2N, and HR1.2Y in the xz -plane. The effect of the supernovae is more drastic for runs HR1.0N, HR1.0Y. This is because most of the massive stars have exploded within a distinct region in the centre of the molecular cloud. However, this effect is clearly seen only in the slices of the midplane ($y=0$). The column density map shows a compact molecular cloud with a slightly tenuous region in its centre. Again, the supernovae result in a redistribution of matter, which is seen by the increased column density at the outer edges of the cloud.

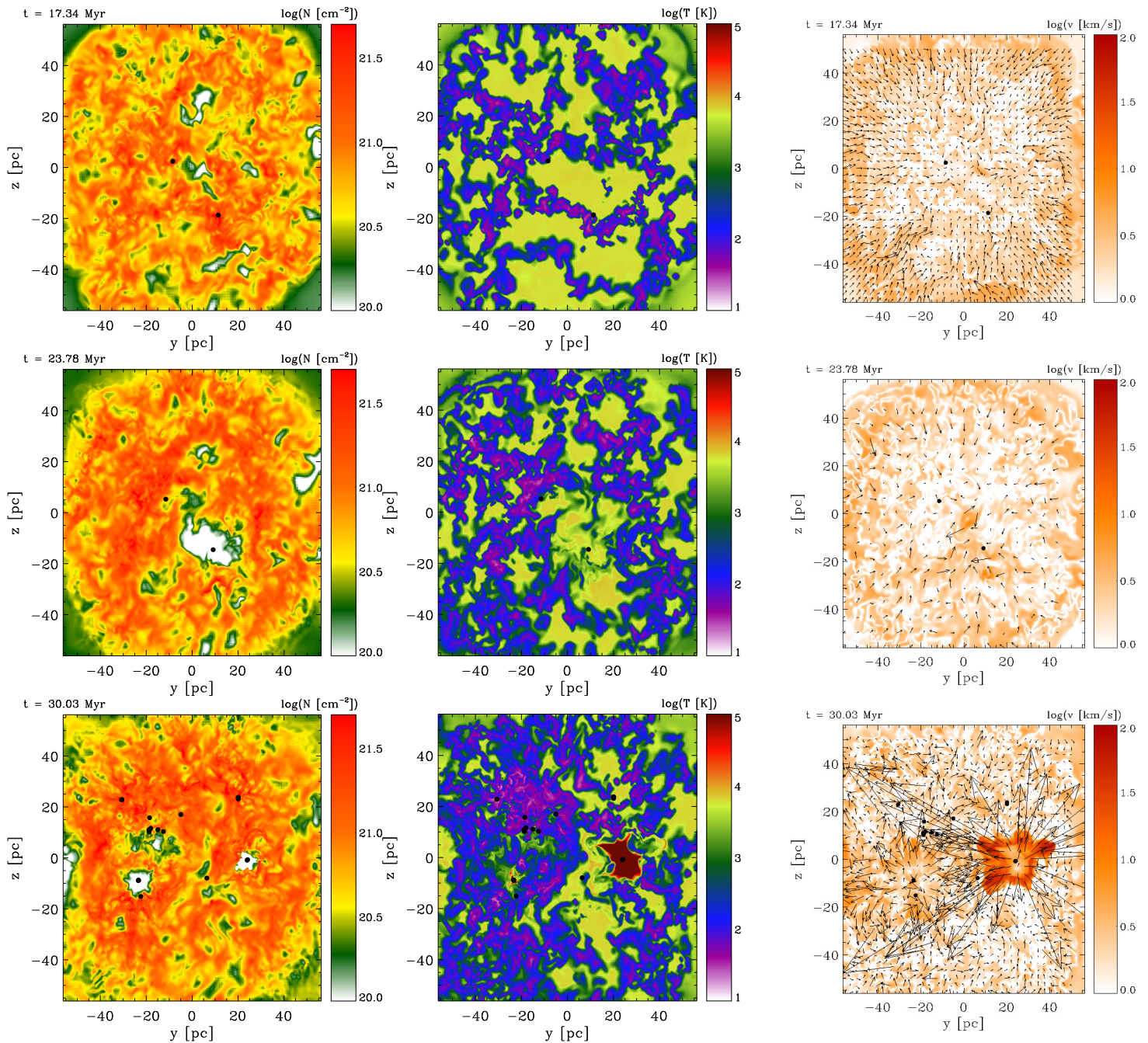


Figure 2. Data of run HR0.8Y. *Left to right:* Column density along the x -axis (parallel to the WNM streams, integration length is 40 pc), temperature, and absolute value of the velocity in the midplane ($x=0$). *Top to bottom:* Different evolutionary stages prior to and after supernova feedback. It is clearly seen that supernovae do not have a huge impact on the cloud dynamics and structure. The effects are only localised to some small regions of a few tens of parsec. In all cases, the typical vector in the velocity plots has a magnitude of $v_{\text{typ}} = 5$ km/s. Note that the vector arrows are plotted with a linear scale. Sink particles are represented by the black dots.

3.2.1 Thermal State of the Cloud

The redistribution of matter on large scales is accompanied by mixing of warm and cold gas on smaller scales. This is because of the turbulence generated by the multiple shock waves interacting with the substructures in the cloud as well as their interaction with each other.

The resulting increase of gas in the thermally unstable regime is seen in figure 4. We show the temporal evolu-

tion of phase diagrams for runs HR0.8N, HR0.8Y, HR1.0N, and HR1.0Y at three different times. The data shown refer to stages prior to, shortly after or long after supernova feedback. In general, the gas evolves along the equilibrium curve, where most of the gas resides in the cold, stable regime. However, a significant part is also detected in the unstable regime, which is material from the halo surrounding the cloud. The scatter around the equilibrium curve is due to turbulent fluctuations in the gas that generate dilatational

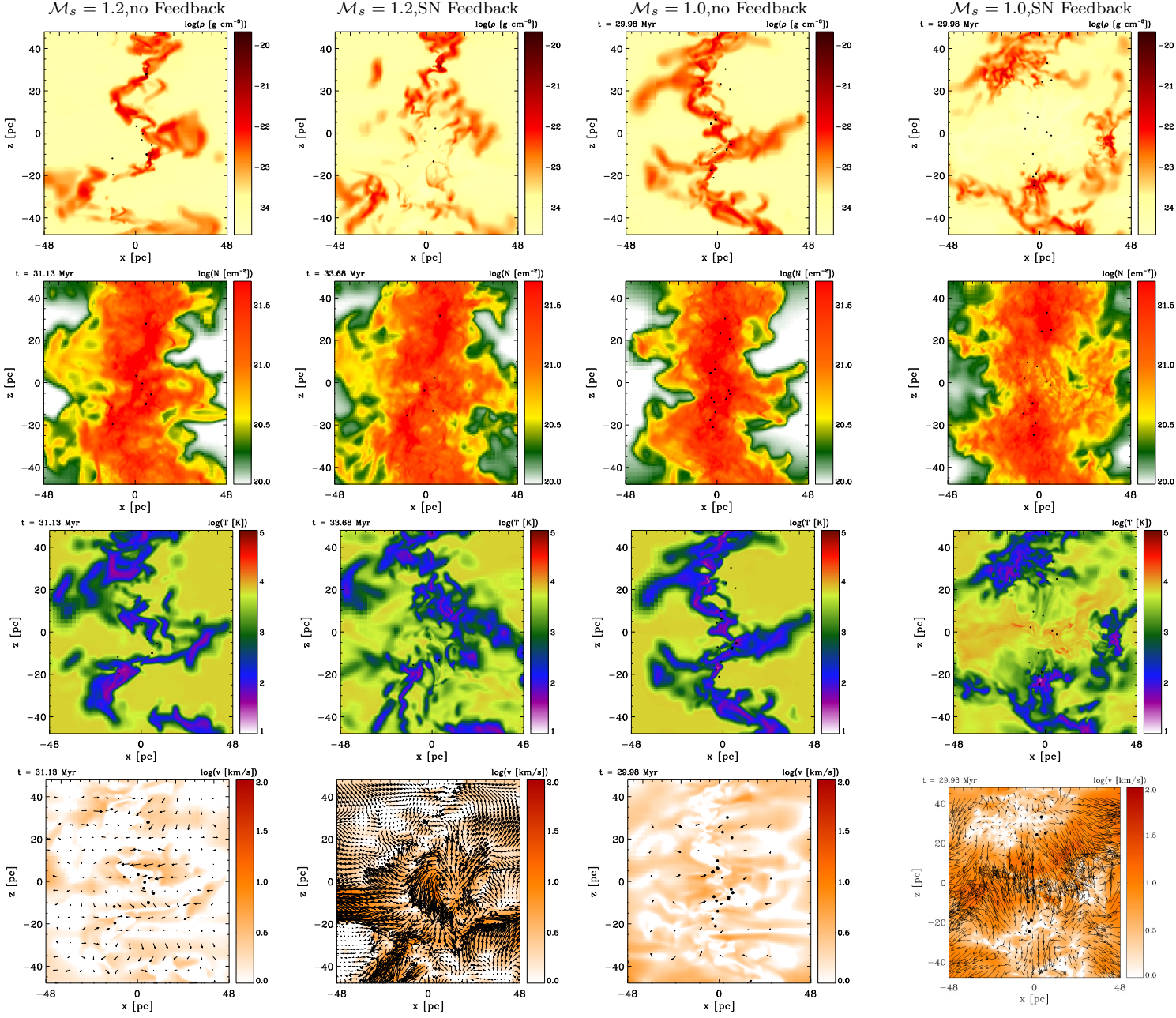


Figure 3. From top to bottom: Density in the $y=0$ -plane (for runs HR1.0) and in the $y=+15$ pc-plane (for runs HR1.2), column density along the y -axis (perpendicular to the WNM streams), temperature, and velocity magnitude. Left two columns for runs HR1.2N and HR1.2Y, respectively. Right two columns for runs HR1.0N and HR1.0Y, respectively. The cloud is dispersed within a localised region. However, the column density map reveals a cloud with a tenuous region in its centre. The latter indicates that supernovae are not able to disrupt the whole cloud. The length of a typical vector is the same as in figure 2. Note that the vector arrows are plotted with a linear scale.

and compressive regions and drive the gas out of the cold and warm *stable* phase into the unstable regime (e.g. Seifried et al. 2011). Even in the case without feedback the pressure scatter increases with time (see the last column of the runs without feedback, i.e. rows one and three). This is a result of global collapse and conversion of gravitational into (turbulent) kinetic energy.

The individual supernovae have a large, but short-lived impact on the phase diagrams. The evolution of the supernova remnant creates over-pressured volumes with high tempera-

tures, as well as under-pressured volumes with very low temperatures. Both phases are primarily seen in the low-density regime. However, the long-term evolution – indicated by a large Δt in the plots – reveals that the gas is cooled faster than it is heated. This is best seen at $t = 24.3$ Myr in run HR0.8Y, where there is only some scatter observed in the under-pressured low-density regime.

The densest parts of the molecular cloud are barely affected. There only occurs a small decrease in mass, because the shock wave is not able to sufficiently disperse these regions.

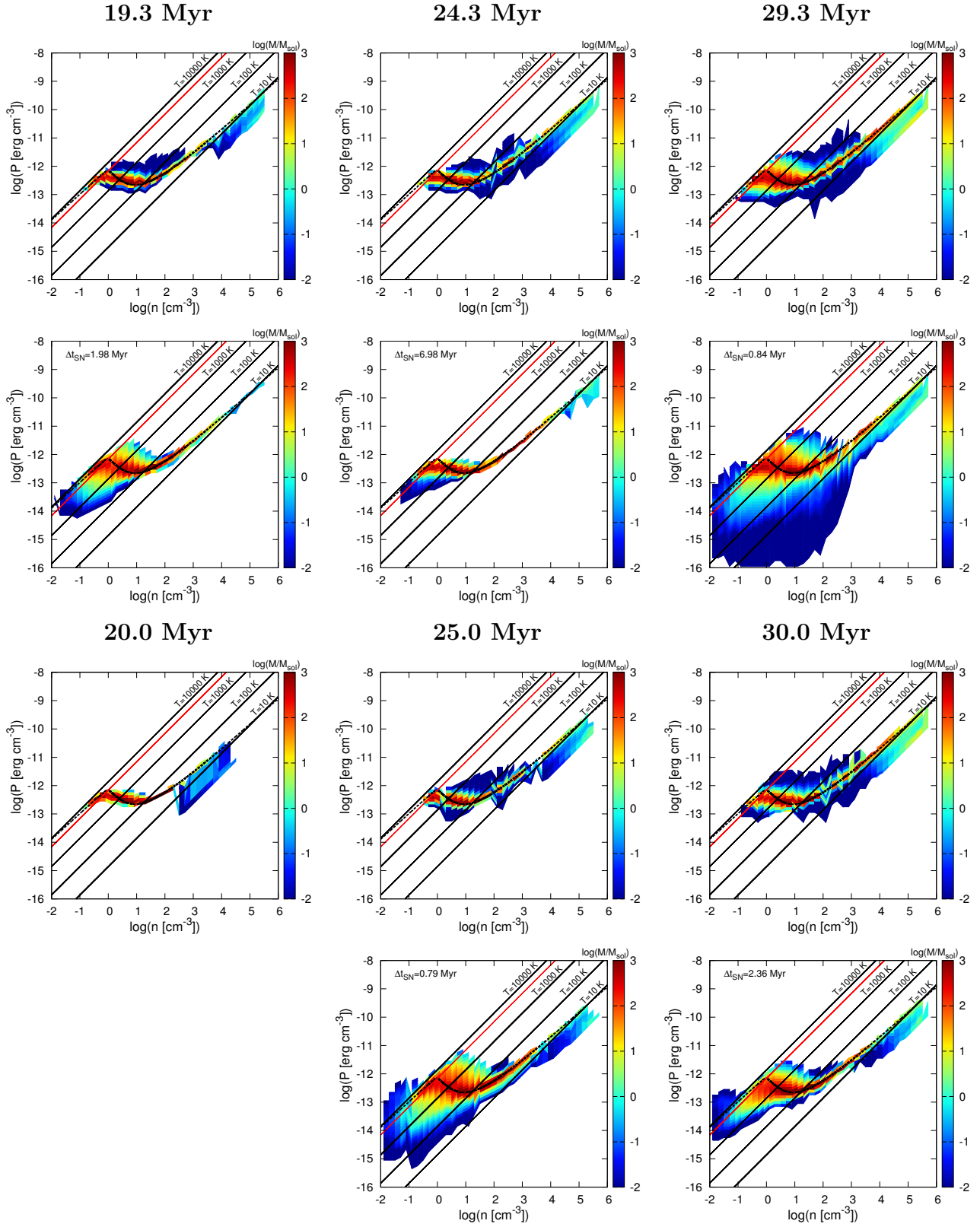


Figure 4. Phase diagrams for the runs HR0.8N,HR0.8Y (top two rows) as well as HR1.0N and HR1.0Y (bottom two rows), respectively, without (upper row) and with (lower row) supernova feedback. Colour coded is the mass in each bin. Also shown are the isotherms for $T = 10, 100, 1000, 10000 \text{ K}$ (solid black lines) and the isotherm for $T = 5000 \text{ K}$ (solid red line). The dashed line marks the equilibrium pressure. The times within some of the plots denote the elapsed time since the last SN. Most of the mass is in the cold phase with the scatter being produced by turbulence. Interestingly, supernovae only produce short-lived strong deviations from pressure equilibrium. After a while the gas approaches equilibrium conditions again. The major difference at later times is the occurrence of a hot gas phase at low densities, which can be attributed to the cavity that has been created by the supernova explosion. Notice that HR1.0N and HR1.0Y are similar at $t = 20 \text{ Myr}$. Hence, we do not show the plot for HR1.0Y.

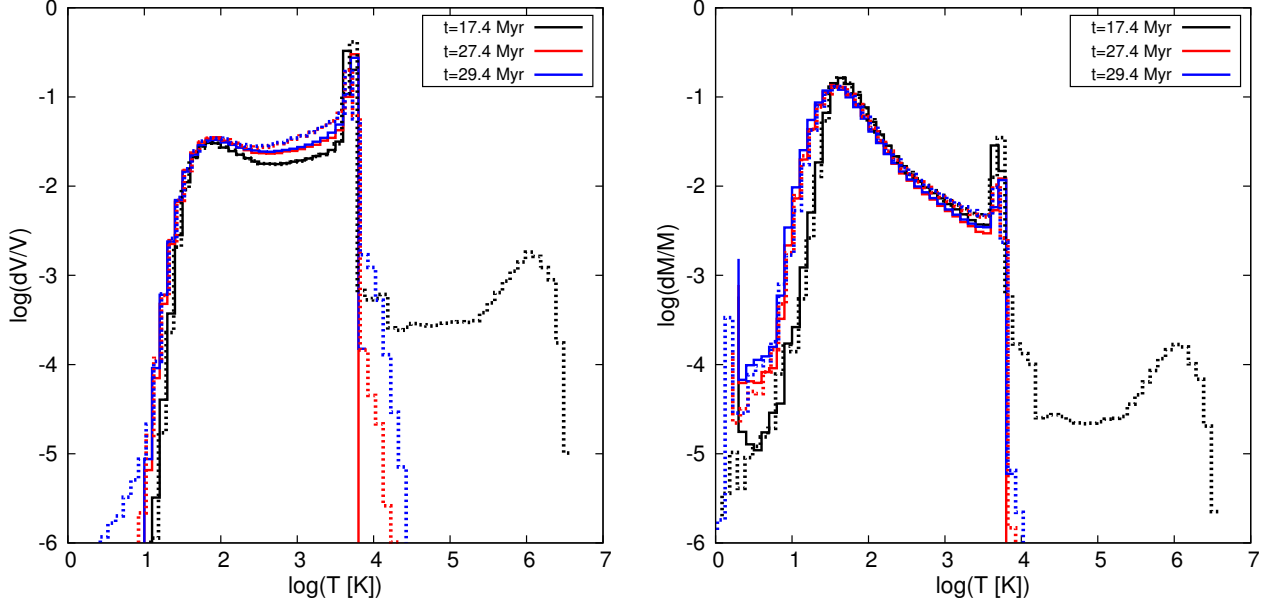


Figure 5. Temperature histogram for different evolutionary stages with (dotted) and without (solid) feedback for runs HR0.8. Note the large increase in temperature due to a supernova explosion (which went off shortly before the shown time). SN feedback results in an increased amount of material in the thermally unstable regime.

In the end of the simulation, the phase diagrams look similar in the intermediate density regime ($10 < n/\text{cm}^{-3} < 100$) for cases with and without feedback in that way that most of the gas evolves along the equilibrium curve. All clouds affected by SN feedback reveal the emergence of low-density ($n \leq 0.1 \text{ cm}^{-3}$), warm material with temperatures of $10^3 - 10^4 \text{ K}$, which can be attributed to the supernova remnants. These regions stay warm for $\sim 7 \text{ Myr}$ (see region between $0 < y/\text{pc} < 20$ and $-40 < z/\text{pc} < 0$ in the temperature slices of figure 2).

In figure 5 we show volume weighted and mass weighted temperature histograms. Most of the mass is in the cold gas. The WNM instead contributes most to the volume fraction. The two major thermodynamic phases of the ISM are clearly identified with temperatures of about $T = 30 - 50 \text{ K}$ for the cold gas and $T \approx 5500 \text{ K}$ for the WNM. A *three-phase* medium is only being generated for a transient period of time, with the additional phase being the hot gas (see also McKee & Ostriker 1977). A more persistent effect is that supernova feedback converts cold gas to gas with moderate temperatures of $2.5 \leq \log(T/\text{K}) \leq 3.5$ with a net increase of $\approx 15\%$ in volume. The mass fraction, however, shows an increase of less than 1% in this temperature regime. We point out that an increase of gas in the thermally unstable regime can also be achieved via turbulent mixing alone (e.g. Seifried et al. 2011).

3.2.2 Long-term dynamical evolution of the dense gas

In figure 6 we show the one-dimensional velocity dispersion (henceforth 1D-dispersion) and thermal pressure of the clouds. The former is calculated in accordance with Gatto et al. (2015, their eqs. (9) and (10)).

In general, the 1D-dispersion is higher for the hydro runs than for the MHD runs, roughly by a factor of 2–3. Hence the ambient magnetic field suppresses velocity fluctuations

by the influence of magnetic pressure and magnetic tension. The single supernova explosions are clearly identified by the sudden increase of the 1D-dispersion. Depending on the density of the region in which the supernovae go off, the 1D-dispersion reaches values of only 12 km/s. However, there are also peaks of only a few km/s in case the SN goes off in regions with high densities. This stage of increased velocity does not last long (up to $\approx 2 \text{ Myr}$). Hence, momentum is not persistently transferred to the dense gas. The decrease in the 1D-dispersion is due to the conversion of kinetic energy into compressive work onto the gas. Additionally, the interaction of the shocks with the collapsing gas yield that the velocities fall below the values of the runs without supernova feedback (compare with the velocity pattern in figure 2). However, for run HR1.0Y there is an obvious net increase in 1D-dispersion by a factor of ≈ 2 . This is due to the formed supernova bubble, which is much more efficient in dispersing the dense gas and driving mixing motions within it² (Sharma et al. 2014).

The evolution of the thermal pressure of the dense gas, $P_{\text{th}} (n > 100 \text{ cm}^{-3})$, is quite similar. The initial thermal pressure is $P_{\text{th,init}} \approx 7 \times 10^{-13} \text{ erg cm}^{-3}$. The compression by the flows and the turbulent fluctuations trigger thermal instability. The isobaric phase of this instability explains the occurrence of dense gas at pressures near the initial value. This phase does not last long and thermal pressure is increased over time. After the flows have deceased ($t \approx 10 \text{ Myr}$), the pressure almost stays constant, indicating the negligible influence of the flows on the thermodynamical state of the cloud.

The individual SN events are clearly identified by the

² Please note that the formation of a supernova bubble is simply because of the clustered sink particles. In this sense, the efficiency of SN feedback in this simulation would change if no bubble was formed.

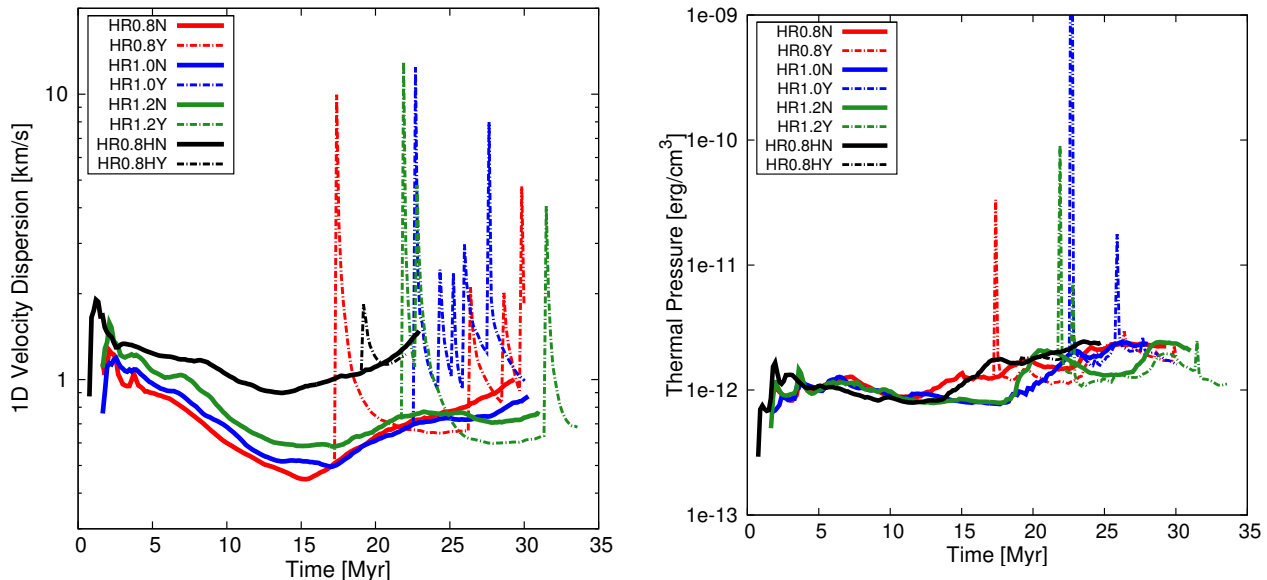


Figure 6. *Left:* Temporal evolution of the RMS velocity of the dense gas for all simulations. The supernovae only temporarily increase the velocity dispersion. This is due to the fact that the dense gas is even more compressed and most of the kinetic energy is hence converted into compressive work. Note that there occur stages where the RMS velocity in the SN runs falls below the no-SN values. Here, global collapse of dense regions towards the centre of the cloud is hampered. *Right:* Evolution of the dense gas’ thermal pressure. The densest parts of the molecular cloud show no significant increase of thermal pressure.

sudden increase. However, most of the thermal energy is radiated away very rapidly. In the end, thermal pressure in the clouds subject to SN feedback approaches the one in the clouds without feedback.

3.2.3 Evolution of energy ratios of the dense gas

Figure 7 shows the evolution of the ratio of kinetic to gravitational energy as well as the ratio of total (thermal plus kinetic) to gravitational energy of the *clouds*. The former ratio is being defined as

$$\alpha = \frac{\frac{1}{2} \sum_i^N \mathcal{V}_i \rho_i |\mathbf{v}_i|^2}{\sum_i^N \mathcal{V}_i \rho_i \Phi_i} = \frac{E_{\text{Kin}}}{E_{\text{Grav}}}, \quad (3)$$

with \mathcal{V}_i being the volume of the i -th cell and N being the number of cells with $n \geq 100 \text{ cm}^{-3}$. Φ_i is the gravitational potential in cell i . The first stage between 0 and 15 Myr is characterised by mass accretion. From 15 Myr on the ratio increases due to the conversion of gravitational energy into kinetic energy due to collapse (Vázquez-Semadeni et al. 2007). Feedback increases the ratio for a small amount of time. During the supernovae the energy budget of the dense gas is purely controlled by kinetic (and thermal) energy. In this time interval, *the cloud seems to be rendered unbound* with $\alpha \geq 2$. However, gravitational energy immediately dominates again. If the time between succeeding supernovae is too long, the ratio drops below the ratio in the cases without feedback. If the time between individual explosions is short (as in case HR1.0Y), the energy input yields a net increase of the ratio. However, there need to be far more supernova explosions in order to achieve (virial) equilibrium stages.

3.3 Star Formation

3.3.1 Number and mass of sink particles

Figure 8 shows the temporal evolution of the total sink particle mass as well as of the number of particles. The sink particles accrete gas and the mass keeps on increasing over time. A decrease in total mass is seen as the initial turbulence is increased, because the accretion rates are influenced by the velocity fluctuations. Additionally, dense regions are more stable against collapse or they are dispersed very quickly. This also results in a smaller number of sink particles in the cloud. Also note the large difference of the particle mass and number in the clouds of the hydrodynamic and MHD case with $\mathcal{M}_{\text{turb}} = 0.8$, indicating the balancing impact of the magnetic field (Vázquez-Semadeni et al. 2011; Hennebelle 2013; Körtgen & Banerjee 2015).

In turn, if supernova feedback is included, the number of sink particles is reduced. Dense regions are dispersed and hence the seeds for sink formation are missing.

The accretion rates are also being reduced by the supernova explosions. This leads to an overall reduction of the total mass, which is of about a factor of two for the MHD runs, but less for the hydro run. The latter is due to the limited simulation duration. Further evolution should show a greater decrease in mass. One interesting aspect concerning the total mass is seen in the evolution. For runs HR0.8Y and HR1.2Y there is a period of nearly constant particle mass, although there exist two sink particles in the cloud. Since only one sink has gone off as a supernova, this indicates that the shock wave swept over the second one. The second sink’s mass supply is being dispersed, thus stopping its accretion either completely or reducing it to very low values. The increase of the mass at later times begins at roughly the same time as the formation of new sinks.

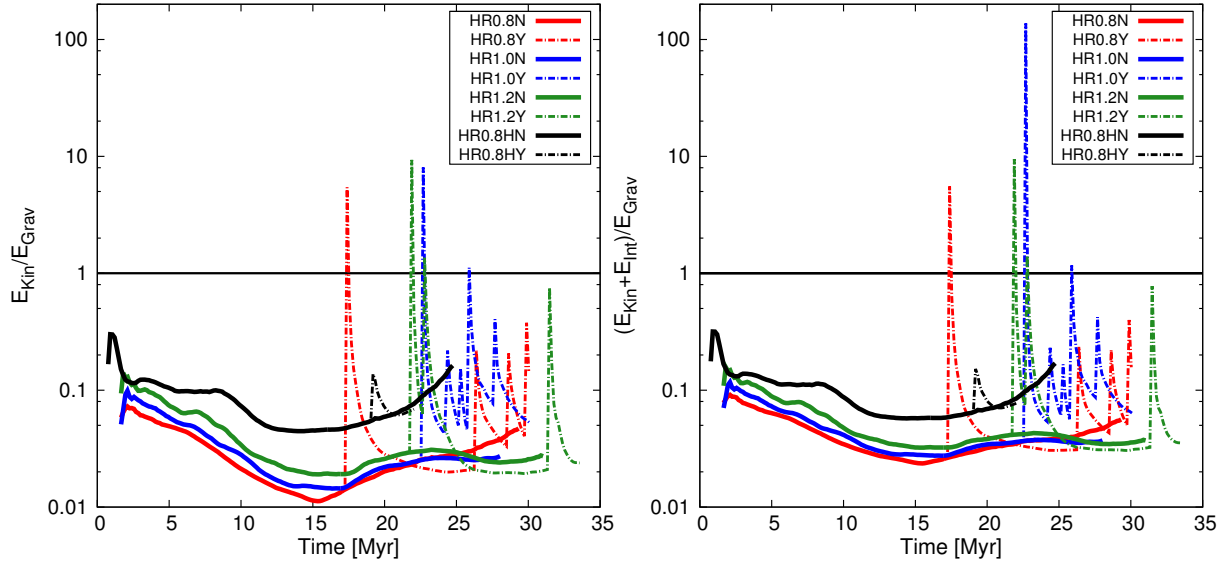


Figure 7. *Left:* Ratio of kinetic to gravitational energy. *Right:* Ratio of kinetic plus thermal to gravitational energy. Only at the time when a supernova goes off, kinetic and thermal energy dominate. The ratio tends to increase with increasing number of supernovae, but it seems to strongly depend on the cloud morphology or the environment where the supernova goes off.

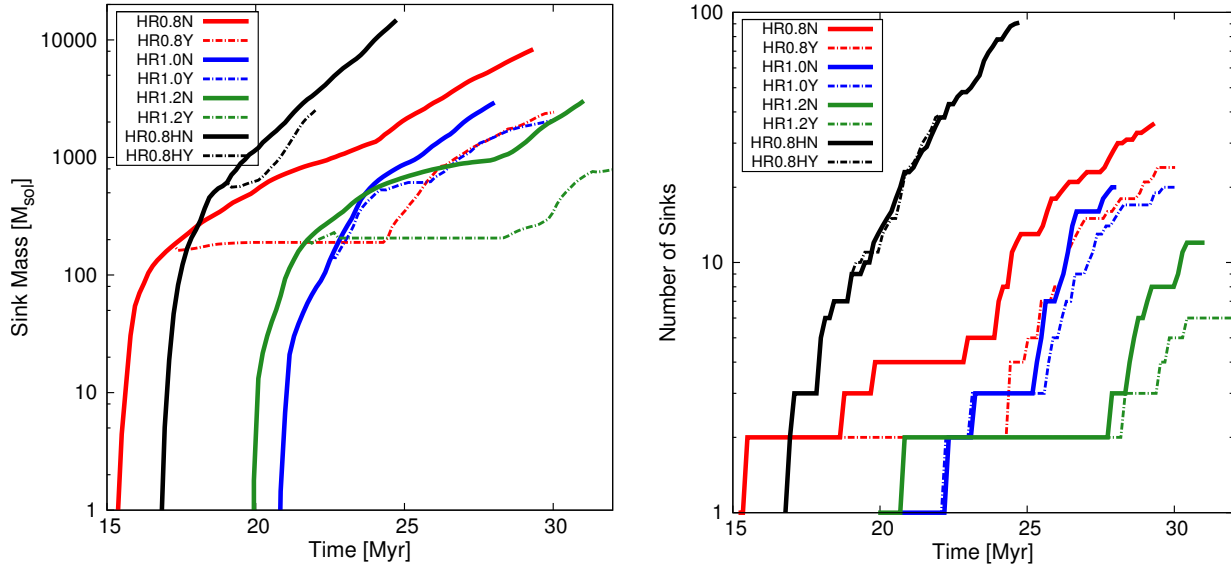


Figure 8. *Left:* Temporal evolution of sink particle mass (solid: without feedback, dash-dotted: with feedback). *Right:* Number of particles (solid: without feedback, dash-dotted: with feedback).

3.3.2 Star Formation Efficiency & Rate

Figure 9 shows the star formation efficiency (SFE), defined as $SFE(t) = M_*(t)/(M_*(t) + M_{\text{cloud}}(t))$, and the temporal derivative of the *total* sink particle mass, which we refer to as star formation rate (SFR), as function of time. In general, both quantities are seen to increase with time. The non-magnetised clouds show a steeper increase of the SFE, as well as of the SFR, at least during the later evolutionary stages, due to the lack of additional magnetic support against gravity (see e.g. Körtgen & Banerjee 2015). The SFE for the magnetised clouds shows a decrease with increasing initial turbulent Mach number. The strong variation for run HR1.2N is due to the increase of the cloud’s mass. This variation is also seen in the other two clouds (HR0.8 and HR1.0),

but in a weaker fashion. In the end, values of 15–20% are obtained.

A similar trend is seen in the SFR. Here, the major difference compared to the hydrodynamic cases is the almost constant evolution for the first 5 to 10 Myr after star formation has begun. The late increase of the SFR is due to global contraction of the cloud, where the magnetic field is not capable of counterbalancing gravity.

If feedback is included, both quantities are significantly decreased. Temporal variations in the accretion properties of both clouds and stars yield reduction efficiencies of factors 2–4. In the end of the simulations, the SFE is reduced by at most a factor of 2. The SFR shows a more pronounced evolution. The supernovae are obviously seen by the sudden decrease in the SFR. The overall impact of supernova feed-

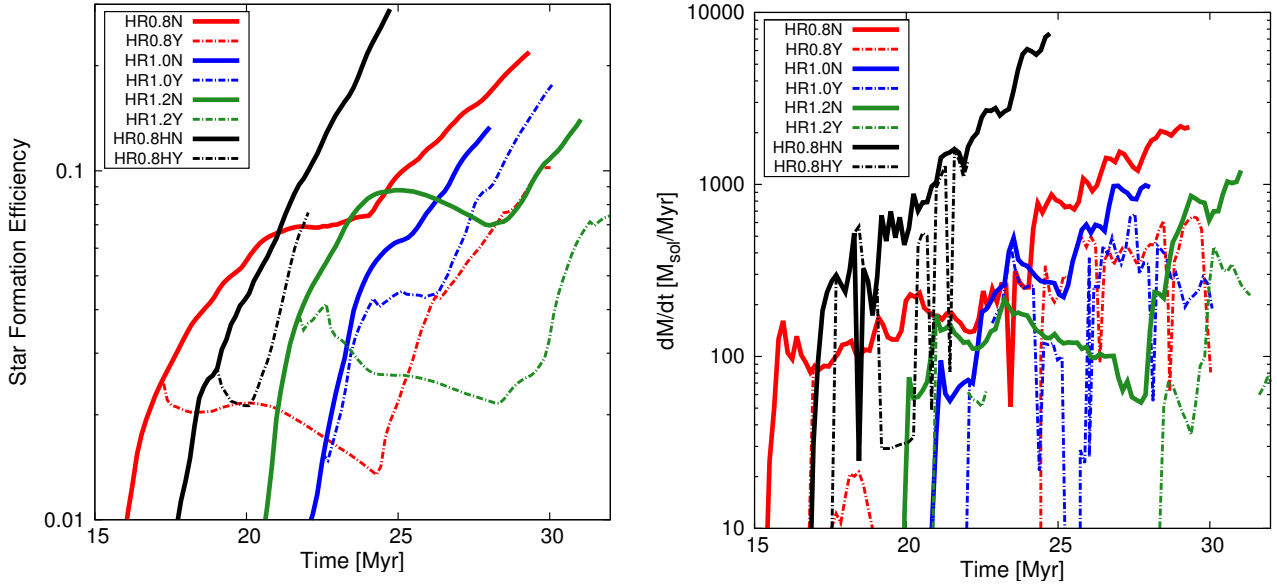


Figure 9. Temporal evolution of the star formation efficiency (left) and corresponding star formation rate (right). Supernova feedback decreases the SFR by about a factor of 2–4. The SFE is only reduced by at most a factor of 2.

back is firstly a reduction and secondly a roughly constant SFR. The former is due to less efficient accretion of the existing sinks as well as suppressed formation of new sinks. The latter is due to the evacuation of dense gas from the centre of the cloud, where most of the sink particles reside. This, in turn, affects the accretion behaviour of the sinks. In the runs without feedback, global collapse increases the amount of gas that can (and will) be accreted by the individual sinks. The SFR is finally being reduced by roughly a factor 2–4.

3.4 The one-dimensional velocity dispersion

Observations of HI in emission indicate that the one-dimensional velocity dispersion of the WNM is $\sigma_{\text{HI}} \approx 10$ km/s (e.g. Heiles & Troland 2003; Tamburro et al. 2009). SN feedback is thought of driving such velocities and models including driven turbulence in the ISM often use these values as the typical turbulent velocity (e.g. Gatto et al. 2015, and references therein). However, as Gatto et al. (2015) report, SN feedback seems to be not capable of driving such high velocity dispersions in HI for longer timescales. Figure 10 shows the one-dimensional velocity dispersion as function of density at the end of each (MHD) simulation, using the recipe given in Gatto et al. (2015, their eqs. (9) and (10))³. As can be seen, velocity dispersions can be as high as ≈ 20 km/s, but only for the low-density gas. The WNM with densities of $0.5 \leq n/\text{cm}^{-3} \leq 5$ reveals values of typically 1.5–5 km/s in clouds subject to SN feedback, far lower than the one observed. The large spread (also for the clouds without feedback) is due to the different accretion properties of the clouds themselves. For run HR0.8Y, there occurred a SN event shortly before the end of the simulation. That is

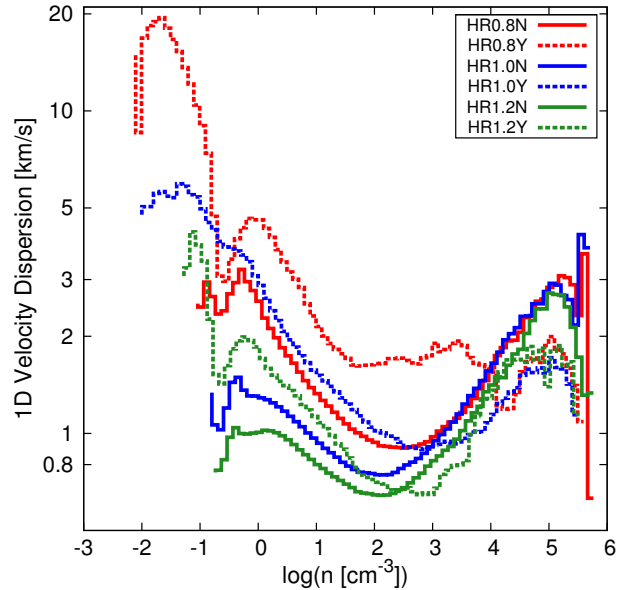


Figure 10. One-dimensional velocity dispersion as function of number density. As is shown, the values fail to reproduce observational results, indicating that SN feedback alone may not be the source of the observed HI dispersion. Note the lower velocity dispersion in the densest parts of the cloud due to stalled gas motions.

why the velocity dispersion is higher compared to HR1.0Y and HR1.2Y. Even for the case of clustered supernovae, the one-dimensional velocity dispersion cannot reproduce observational results.

3.5 Lifetimes of individual regions within the clouds

In order to evaluate the efficiency of SNe in disrupting small regions within molecular clouds, we give a comparative

³ Note that we do not include different chemical species. Thus the velocity dispersion is for one fluid and we compare our WNM regime with the HI emission results.

Table 2. Estimated diameter and destruction timescale for different feedback mechanisms.

Source	Diameter (pc)	Timescale	Form of Feedback
HR0.8Y ^a	4.8	29 kyr	SN
HR1.0Y ^a	9.7	50 kyr	SN
HR1.2Y ^a	6.5	14 kyr	SN
Rogers & Pittard (2013)	8	<1.5 Myr	SN
Colín et al. (2013)	10	10–20 Myr	Ionisation
Dale et al. (2014) ^b	10	10–20 Myr	Ionisation
Martizzi et al. (2015) ^c	10	15 kyr	SN

^aThis study.

^bDale et al. (2014) give the size of the region, but do not give a concrete destruction timescale. However, they argue that their timescales are comparable to Vázquez-Semadeni et al. (2010).

^cThe size of the region is read off by eye from their figure 1.

overview in table 2. SN feedback is much more efficient in disrupting embedded structures like clumps and cores since the timescales (derived from simulation data: Estimate of cavity size at a timestep t after a SN has gone off.) for the disruption are roughly an order of magnitude smaller than for ionisation feedback. Our results are in good agreement with the study by Martizzi et al. (2015), who carried out simulations of individual SNe going off in an inhomogeneous medium. However, our achieved timescales are somewhat larger, because on the one hand, they did not include a magnetic field. On the other hand, the densities within our clumps, in which the massive stars explode, might be higher by up to two orders of magnitude. Hence, radiative cooling is much more efficient in our simulations. In contrast, Rogers & Pittard (2013) give larger timescales for the disruption of a clump by SN feedback of approximately 1.5 Myr, although the authors have included feedback mechanisms prior to the SN.

4 DISCUSSION

4.1 Limitations

We point out that our simulations lack the progenitor feedback mechanisms like stellar winds and the star’s ionising radiation. In order to estimate the impact of progenitor feedback, one can calculate the cooling timescale

$$t_c = \frac{3}{2} \frac{k_B T}{n \Lambda(T)}. \quad (4)$$

Here, k_B is Boltzmann’s constant, T is temperature, n is the number density of the heated gas, and $\Lambda(T)$ is the temperature dependent cooling function, respectively. t_c then gives the timescale when cooling starts to become dominant. For our simulations, typical densities in the stellar environment are in the range $n \in [10^2, 10^5] \text{ cm}^{-3}$ and the SN temperatures are as high as $T = 10^7 - 10^8 \text{ K}$. The cooling function at these temperatures is roughly constant ($\Lambda(T) \approx 5 \times 10^{-23} \text{ erg cm}^3 \text{ s}^{-1}$). These values give $t_c (T = 10^7 \text{ K}) = 1.3 \times 10^{-5} - 1.3 \times 10^{-2} \text{ Myr}$ and $t_c (T = 10^8 \text{ K}) = 1.3 \times 10^{-4} - 1.3 \times 10^{-1} \text{ Myr}$, which are still larger than the dynamical timescale, as stated in section 2.3. Hence, the major part of the injected thermal energy is radiated away within only a few timesteps. The resulting heating

of parts of the molecular cloud is then due to shock heating and the dispersion of gas clumps is driven by momentum input. In contrast, if the massive star generates a large HII region, the SN will go off in a region of tenuous gas with densities of the order of $n_{\text{HII}} = 0.1 - 1 \text{ cm}^{-3}$. The cooling timescale then increases to $t_c (T = 10^7 \text{ K}) = 1.3 - 13 \text{ Myr}$ and $t_c (T = 10^8 \text{ K}) = 13 - 130 \text{ Myr}$, respectively. The SN remnant is hence only subject to adiabatic cooling and should expand much further due to its pressure-driven evolution up to the point where the SN remnant hits the shell that was being swept-up by the HII region. The combined effects of ionising radiation and SN should then be able to disrupt entire molecular clouds on timescales less than that for pure ionising feedback, that is, of the order of a few Myr. This is also in agreement with the study by Sharma et al. (2014), who showed that superbubbles can retain up to 40% of their energy over longer timescales, in stark contrast to the failure of individual SNe. We here point out that recently Walch & Naab (2015) concluded that the combined effects of ionisation and SNe are *not* capable of disrupting molecular clouds. The authors note that the HII region will generate regions of reduced density as well as regions where the density is increased due to compression. This will, on the one hand, help the SNe to disrupt parts of the cloud, but on the other hand is able to generate obstacles (due to gas compression) for the remnant where its evolution is stalled. The whole process will enhance the impact of the SNe by only 50%. Note, however, that their total cloud mass is approximately an order of magnitude larger than the cloud masses discussed in this study. It is therefore possible that their results change with varying cloud mass. The latter has recently been investigated by Dale et al. (2014). The authors find that ionising radiation is capable of disrupting large parts of clouds with masses of $M_{\text{cloud}} \approx 10^4 M_{\odot}$, but fails to disrupt clouds with masses of $M_{\text{cloud}} \approx 10^6 M_{\odot}$. The influence of the massive stars is enhanced when stellar winds are included. Please note further that our failure to fully disrupt the clouds with SNe alone, and our proposal that possibly the combined action of ionising radiation and SNe may accomplish this task, should not be confused with the above mentioned results by Dale et al. (2014, see also Dale et al. (2012)). In their case, it is possible that the difficulty in destroying such clouds arises by the initial conditions considered by those authors (initially spherical clouds), since

the spherical geometry causes the deepest possible potential wells, while real clouds are more likely sheetlike or filamentary (e.g. Bally 2001; Heiles & Troland 2003) as is the case of the cloud in our simulations. In our case, the inability of the SNe alone to destroy the clouds is due more to its brief, impulsive nature, and the combination of this kind of feedback with ionising radiation may well be capable of destroying even very massive clouds. We plan to address this question in a future study.

4.2 Time duration of the simulations

We ran the simulations for a maximum time of $t \sim 35$ Myr. During this time the molecular clouds are not fully disrupted, hence star formation continues throughout. As reviewed by Blitz et al. (2007), observations of molecular clouds indicate life times of 20–30 Myr⁴ in agreement with our simulations. We thus argue that this time span is enough to study star formation and stellar feedback effects in single, isolated clouds.

5 SUMMARY

In this study we have presented results from numerical simulations on molecular cloud evolution including supernova feedback from massive stars.

The results suggest that supernova feedback alone is not sufficient to disrupt molecular clouds, consistent with previous studies. The dispersal is only restricted to some fraction of the parental cloud. Though the efficiency in disrupting the cloud is very low, supernovae still create regions of moderate temperature, which affects the thermodynamic behaviour of the gas. The efficiency also strongly depends on where the supernovae go off, on the number of supernova events, as well as on the clumpiness of the cloud. Single supernovae initially show signs of compression, which might lead to triggered star formation. With time, the shocks disperse those regions and the net effect is a negative feedback (disruption). If the supernovae are clustered, their combined energy and momentum input is sufficient to disrupt larger amounts of the parental cloud. However, even with clustered supernovae, the cloud is not fully destroyed. The supernovae are still able to remove up to 50% of the total cloud mass. The inhomogeneity of the cloud due to initial turbulent fluctuations enables energy from the SN to escape through low-density channels. On the other hand, more turbulent clouds are also less compact and the substructures are hence dispersed more easily.

The suppression of star formation, however, is quite effective with reduction of the SFE and SFR by factors of 2–4, again consistent with previous studies on SN feedback. This is due to the fact that there occurs a short-period, but sufficient momentum transfer to the dense gas, which leads to its dispersion. However, our results indicate that star formation is not halted and continues throughout the simulation ($t \sim 35$ Myr) in all cases.

ACKNOWLEDGEMENTS

We thank an anonymous referee for his/her comments, which helped to improve the quality of this study. BK acknowledges hospitality at Centro de Radioastronomía y Astrofísica, Universidad Nacional Autónoma México, during the initial stages of this study and Gilberto C. Gómez for stimulating discussions. DS acknowledges funding by the Bonn-Cologne Graduate School as well as the Deutsche Forschungsgemeinschaft (DFG) via the Sonderforschungsbereich SFB 956 Conditions and Impact of Star Formation. RB acknowledges funding by the DFG via the Emmy-Noether grant BA 3706/1-1, the ISM-SPP 1573 grants BA 3706/3-1 and BA 3706/3-2, as well as for the grant BA 3706/4-1. The simulations were run on HLRN-III under project grant hhp00022. The authors also gratefully acknowledge the Gauss Centre for Supercomputing e.V. (www.gauss-centre.eu) for funding this project (project-id: pr85ga) by providing computing time on the GCS Supercomputer SuperMUC at Leibniz Supercomputing Centre (LRZ, www.lrz.de). The authors furthermore gratefully acknowledge the Gauss Centre for Supercomputing (GCS) for providing computing time through the John von Neumann Institute for Computing (NIC) on the GCS share of the supercomputer JUQUEEN⁵ at Jülich Supercomputing Centre (JSC). GCS is the alliance of the three national supercomputing centres HLRS (Universität Stuttgart), JSC (Forschungszentrum Jülich), and LRZ (Bayerische Akademie der Wissenschaften), funded by the German Federal Ministry of Education and Research (BMBF) and the German State Ministries for Research of Baden-Württemberg (MWK), Bayern (StMWFK) and Nordrhein-Westfalen (MIWF). The software used in this work was in part developed by the DOE-supported ASC/Alliance Center for Astrophysical Thermonuclear Flashes at the University of Chicago.

REFERENCES

- Bally, J. 2001, in *Astronomical Society of the Pacific Conference Series*, Vol. 231, *Tetons 4: Galactic Structure, Stars and the Interstellar Medium*, ed. C. E. Woodward, M. D. Bica, & J. M. Shull, 204–+
- Banerjee, R., Klessen, R. S., & Fendt, C. 2007, *ApJ*, 668, 1028
- Banerjee, R., Vázquez-Semadeni, E., Hennebelle, P., & Klessen, R. S. 2009, *MNRAS*, 398, 1082
- Blitz, L., Fukui, Y., Kawamura, A., et al. 2007, *Protostars and Planets V*, 81
- Bouchut, F., Klingenberg, C., & Waagan, K. 2007, *Numerische Mathematik*, 108, 7
- Bouchut, F., Klingenberg, C., & Waagan, K. 2009, *Numerische Mathematik*, accepted
- Chen, C.-Y. & Ostriker, E. C. 2014, *ApJ*, 785, 69
- Colín, P., Vázquez-Semadeni, E., & Gómez, G. C. 2013, *MNRAS*, 435, 1701

⁵ Jülich Supercomputing Centre. (2015). JUQUEEN: IBM Blue Gene/Q Supercomputer System at the Jülich Supercomputing Centre. *Journal of large-scale research facilities*, 1, A1. <http://dx.doi.org/10.17815/jlsrf-1-18>

⁴ Though having an uncertainty of $\sim 50\%$.

- Dale, J. E., Ercolano, B., & Bonnell, I. A. 2012, *MNRAS*, 424, 377
- Dale, J. E., Ngoumou, J., Ercolano, B., & Bonnell, I. A. 2013, *MNRAS*, 436, 3430
- Dale, J. E., Ngoumou, J., Ercolano, B., & Bonnell, I. A. 2014, *MNRAS*, 442, 694
- de Avillez, M. A. 2000, *MNRAS*, 315, 479
- de Avillez, M. A. & Breitschwerdt, D. 2004, *A&A*, 425, 899
- de Avillez, M. A. & Mac Low, M.-M. 2002, *ApJ*, 581, 1047
- Dubey, A., Fisher, R., Graziani, C., et al. 2008, in *Astronomical Society of the Pacific Conference Series*, Vol. 385, *Numerical Modeling of Space Plasma Flows*, ed. N. V. Pogorelov, E. Audit, & G. P. Zank, 145–+
- Federrath, C., Banerjee, R., Clark, P. C., & Klessen, R. S. 2010, *ApJ*, 713, 269
- Federrath, C. & Klessen, R. S. 2012, *ApJ*, 761, 156
- Federrath, C. & Klessen, R. S. 2013, *ApJ*, 763, 51
- Fryxell, B., Olson, K., Ricker, P., et al. 2000, *ApJS*, 131, 273
- Gatto, A., Walch, S., Mac Low, M.-M., et al. 2015, *MNRAS*, 449, 1057
- Geen, S., Rosdahl, J., Blaizot, J., Devriendt, J., & Slyz, A. 2015, *MNRAS*, 448, 3248
- Gent, F. A., Shukurov, A., Fletcher, A., Sarson, G. R., & Mantere, M. J. 2013a, *MNRAS*, 432, 1396
- Gent, F. A., Shukurov, A., Sarson, G. R., Fletcher, A., & Mantere, M. J. 2013b, *MNRAS*, 430, L40
- Girichidis, P., Walch, S., Naab, T., et al. 2015, *ArXiv e-prints*
- Gritschneider, M., Naab, T., Walch, S., Burkert, A., & Heitsch, F. 2009, *ApJ*, 694, L26
- Heiles, C. & Troland, T. H. 2003, *ApJ*, 586, 1067
- Heitsch, F., Burkert, A., Hartmann, L. W., Slyz, A. D., & Devriendt, J. E. G. 2005, *ApJ*, 633, L113
- Heitsch, F., Hartmann, L., & Burkert, A. 2008, *ArXiv e-prints*, 805
- Hennebelle, P. 2013, *A&A*, 556, A153
- Hennebelle, P. & Iffrig, O. 2014, *A&A*, 570, A81
- Hill, A. S., Jounge, M. R., Mac Low, M.-M., et al. 2012, *ApJ*, 750, 104
- Iffrig, O. & Hennebelle, P. 2015, *A&A*, 576, A95
- Jounge, M. K. R. & Mac Low, M.-M. 2006, *ApJ*, 653, 1266
- Jounge, M. K. R. & Mac Low, M.-M. 2007, in *IAU Symposium*, Vol. 237, *IAU Symposium*, ed. B. G. Elmegreen & J. Palous, 358–362
- Jounge, M. R., Mac Low, M.-M., & Bryan, G. L. 2009, *ApJ*, 704, 137
- Kim, C.-G. & Ostriker, E. C. 2015, *ApJ*, 802, 99
- Korpi, M. J., Brandenburg, A., Shukurov, A., Tuominen, I., & Nordlund, Å. 1999, *ApJ*, 514, L99
- Körtgen, B. & Banerjee, R. 2015, *MNRAS*, 451, 3340
- Koyama, H. & Inutsuka, S.-I. 2000, *ApJ*, 532, 980
- Kroupa, P. 2001, *MNRAS*, 322, 231
- Li, H., Li, D., Qian, L., et al. 2015a, *ArXiv e-prints*
- Li, M., Ostriker, J. P., Cen, R., Bryan, G. L., & Naab, T. 2015b, *ApJ*, 814, 4
- Mac Low, M.-M. & Klessen, R. S. 2004, *Reviews of Modern Physics*, 76, 125
- Martizzi, D., Faucher-Giguère, C.-A., & Quataert, E. 2015, *MNRAS*, 450, 504
- McKee, C. F. & Ostriker, J. P. 1977, *ApJ*, 218, 148
- Nakamura, F. & Li, Z.-Y. 2014, *ApJ*, 783, 115
- Nakano, T. & Nakamura, T. 1978, *PASJ*, 30, 671
- Ostriker, E. C. & Shetty, R. 2011, *ApJ*, 731, 41
- Padoan, P., Bally, J., Billawala, Y., Juvella, M., & Nordlund, Å. 1999, *ApJ*, 525, 318
- Padoan, P. & Nordlund, Å. 1999, *ApJ*, 526, 279
- Pittard, J. M. & Rogers, H. 2012, in *Astronomical Society of the Pacific Conference Series*, Vol. 465, *Astronomical Society of the Pacific Conference Series*, ed. L. Drissen, C. Rubert, N. St-Louis, & A. F. J. Moffat, 398
- Robitaille, T. P. & Whitney, B. A. 2010, *ApJ*, 710, L11
- Rogers, H. & Pittard, J. M. 2013, *MNRAS*, 431, 1337
- Rosen, A. & Bregman, J. N. 1995, *ApJ*, 440, 634
- Sedov, L. I. 1959, *Similarity and Dimensional Methods in Mechanics*
- Seifried, D., Schmidt, W., & Niemeyer, J. C. 2011, *A&A*, 526, A14
- Sharma, P., Roy, A., Nath, B. B., & Shchekinov, Y. 2014, *MNRAS*, 443, 3463
- Shetty, R. & Ostriker, E. C. 2008, *ApJ*, 684, 978
- Shetty, R. & Ostriker, E. C. 2012, *ApJ*, 754, 2
- Tamburro, D., Rix, H.-W., Leroy, A. K., et al. 2009, *AJ*, 137, 4424
- Tammann, G. A., Loeffler, W., & Schroeder, A. 1994, *ApJS*, 92, 487
- Tasker, E. J., Wadsley, J., & Pudritz, R. 2015, *ApJ*, 801, 33
- Tuelove, J. K., Klein, R. I., McKee, C. F., et al. 1997, *ApJ*, 489, L179+
- Vázquez-Semadeni, E., Banerjee, R., Gómez, G. C., et al. 2011, *MNRAS*, 414, 2511
- Vázquez-Semadeni, E., Colín, P., Gómez, G. C., Ballesteros-Paredes, J., & Watson, A. W. 2010, *ApJ*, 715, 1302
- Vázquez-Semadeni, E., Gómez, G. C., Jappsen, A. K., et al. 2007, *ApJ*, 657, 870
- Vishniac, E. T. 1994, *ApJ*, 428, 186
- Waagan, K., Federrath, C., & Klingenberg, C. 2011, *Journal of Computational Physics*, 230, 3331
- Walch, S. & Naab, T. 2015, *MNRAS*, 451, 2757
- Walch, S., Whitworth, A. P., Bisbas, T. G., Wünsch, R., & Hubber, D. A. 2013, *MNRAS*, 435, 917
- Walch, S. K., Girichidis, P., Naab, T., et al. 2014, *ArXiv e-prints*
- Walch, S. K., Whitworth, A. P., Bisbas, T., Wünsch, R., & Hubber, D. 2012, *MNRAS*, 427, 625
- Wang, P., Li, Z., Abel, T., & Nakamura, F. 2010, *ApJ*, 709, 27
- Weigert, A., Wendker, H. J., & Wisotzki, L. 2009, *Astronomie und Astrophysik (Wiley-VCH 2009)*

APPENDIX A: RESOLUTION STUDY: SINK PARTICLES

As stated in section 2.3, supernova feedback is only enabled if the total sink particle mass exceeds $M_{\text{Kroupa}} = 160 M_{\odot}$. Figure A1 shows the total mass of stars for three simulations with varying numerical resolution. The Kroupa-mass (horizontal solid black line) is reached at different times. However, the temporal difference is not significant for the global evolution of the cloud since it is only about 1 Myr. With time, the total stellar mass converges. It is thus independent of

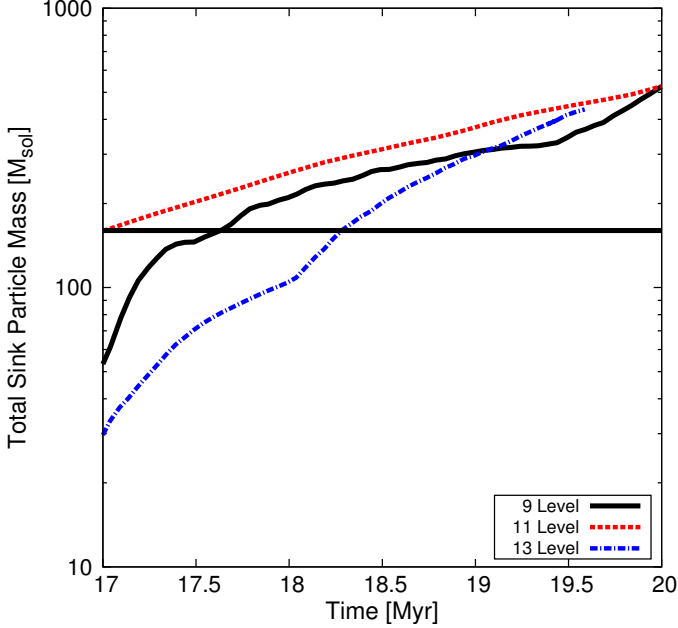


Figure A1. Resolution study showing the mass of all sink particles as function of time for a time interval of $\Delta t \approx 3$ Myr. The horizontal black line denotes the critical cluster-mass for having at least one massive star. The temporal difference for reaching the critical mass is about $t_{\text{diff}} \approx 1.2$ Myr. It is thus not significant for the long-term dynamical evolution of the cloud. The total mass in all sink particles converges after some Myr of evolution.

the numerical resolution. The usage of our IMF-fitting approach then gives the same supernova features for different resolutions. Note that the initial stages of the sink particle evolution differ due to different threshold densities. These densities influence the formation of sink particles as well as their accretion behaviour (gas is only accreted onto the sink particle, if the density in the respective cells exceeds the threshold density).

APPENDIX B: RESOLUTION STUDY: SUPERNOVA REMNANT

Sufficient numerical resolution of the supernova remnant is crucial for its further evolution. However, using too many cells may lead to undesired effects on the environment of the exploding sink particle. In figure B1 we compare two simulations in which the radius of the remnant is resolved with 2 grid cells (Low-Res in the figure; our fiducial value) and with 10 cells (High-Res). Shown is the evolution of the total (thermal plus kinetic) energy of the gas. For this resolution study, the simulation is stopped a few Myr after the first SN has gone off. As can be seen, only minor deviations occur at the time of energy injection. The total energy injected in the fiducial run reaches $\sim 9.5 \times 10^{50}$ erg. These deviations from the model value (10^{51} erg) are due to the small number of cells for resolving a spherical supernova remnant with cubic grid cells. However, the long-term evolution shows no significant difference (the deviations are $\leq 1\%$) and we conclude that the radius of the remnant is sufficiently resolved with 2 grid cells.

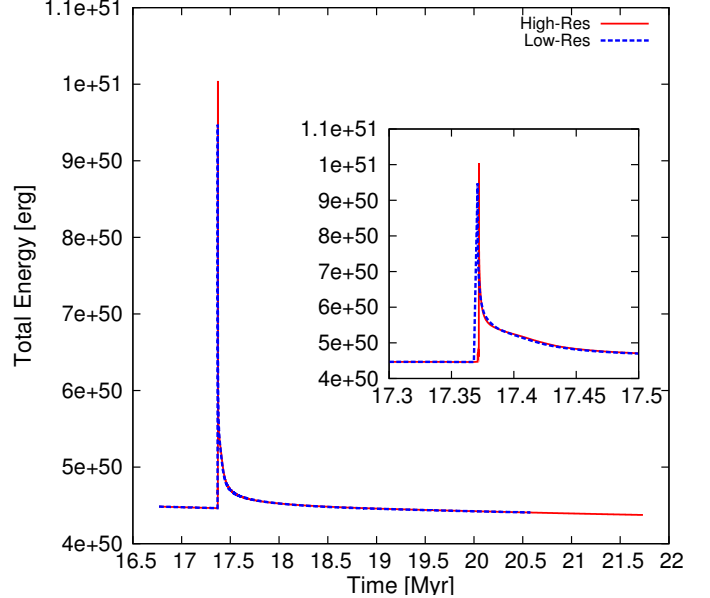


Figure B1. Resolution study showing the temporal evolution of the total (thermal+kinetic) energy of run HR0.8Y. We compare two ways of resolving the radius of the supernova remnant. Our fiducial run uses two cells for resolving the SNR (termed *Low-Res*) and the control simulation resolves the SNR with ten grid cells (termed *High-Res*). It is seen that the evolution is quite similar and that our fiducial value of 2 grid cells is sufficient.

APPENDIX C: NOTES ON THE SUPERNOVA RATE

We use a supernova rate (in terms of *supernovae per solar mass*) as a combination of the observed supernova rate (in terms of *supernovae per year*) and the Galactic star formation rate (in terms of *solar mass per year*). This gives

$$SNR_M(\#/M_\odot) = \frac{SNR_{\text{yr}}(\#/yr)}{SFR(M_\odot/yr)}. \quad (\text{C1})$$

Using values for $SNR_{\text{yr}} = (44 \text{ yr})^{-1}$ from (Tammann et al. 1994) and $SFR = 1 M_\odot \text{ yr}^{-1}$ from (Mac Low & Klessen 2004), the supernova rate becomes

$$SNR_M = (44 M_\odot)^{-1}. \quad (\text{C2})$$

This is analogous to a calculation of the supernova rate directly from an IMF. Using an IMF, SNR_M is just the number of massive stars per unit solar mass. For a Kroupa-IMF $SNR_M = (100 M_\odot)^{-1} - (160 M_\odot)^{-1}$, depending on the detailed numerical constants. The SNR in this study is hence three to four times higher than those from IMF estimates and thus gives an upper limit on the efficiency of cloud dispersion and disruption by supernovae.

For comparison, Joung & Mac Low (2006) and Gatto et al. (2015) use the rate from Tammann et al. (1994) and scale it down to the respective size of the simulation box (compared to the area of the Galaxy). This gives

$$SNR_{256 \times 256 \text{ pc}^2} = 2 \text{ SNe/Myr}. \quad (\text{C3})$$

Knowing the number of SNe and the time interval in which they are going off, we are able to calculate a SN-rate in terms of *supernovae per Myr*. The results give $SNR_{\text{Myr}} \approx 1.7 \text{ SNe/Myr} - 2.1 \text{ SNe/Myr}$ in very good agreement with the above mentioned studies.